Zn^{2+} Sensitivity of High- and Low-Voltage Activated Calcium Channels

Hong-Shuo Sun, Kwokyin Hui, David W. K. Lee, and Zhong-Ping Feng
Department of Physiology, University of Toronto, Toronto, Ontario, Canada

ABSTRACT The essential cation zinc (Zn^{2+}) blocks voltage-dependent calcium channels in several cell types, which exhibit different sensitivities to Zn^{2+}. The specificity of the Zn^{2+} effect on voltage-dependent calcium channel subtypes has not been systematically investigated. In this study, we used a transient protein expression system to determine the Zn^{2+} effect on low- and high-voltage activated channels. We found that in Ba^{2+}, the IC_{50} value of Zn^{2+} was α_1-subunit-dependent with lowest value for $Ca_V1.2$, and highest for $Ca_V3.1$; the sensitivity of the channels to Zn^{2+} was approximately ranked as $Ca_V1.2 > Ca_V3.2 > Ca_V2.3 > Ca_V2.2 = Ca_V 2.1 \geq Ca_V3.3 = Ca_V3.1$. Although the $Ca_V2.2$ and $Ca_V3.1$ channels had similar IC_{50} for Zn^{2+} in Ba^{2+}, the $Ca_V2.2$, but not $Ca_V3.1$ channels, had ~10-fold higher IC_{50} to Zn^{2+} in Ca^{2+}. The reduced sensitivity of $Ca_V2.2$ channels to Zn^{2+} in Ca^{2+} was partially reversed by disrupting a putative EF-hand motif located external to the selectivity filter EEEE locus. Thus, our findings support the notion that the Zn^{2+} block, mediated by multiple mechanisms, may depend on conformational changes surrounding the α_1 pore regions. These findings provide fundamental insights into the mechanism underlying the inhibitory effect of zinc on various Ca^{2+} channel subtypes.

INTRODUCTION

The regulation of calcium entry into cells via voltage-dependent calcium channels (VDCCs) plays a fundamental role in controlling synaptic transmission, membrane excitability, muscle contraction, rhythmic activity, gene transcription, and signal transduction pathways (1,2). Therefore, elucidating the molecular mechanisms regulating calcium channel conductivity is essential for a greater comprehension of cell biology.

Zinc, an essential transition divalent cation, is involved in maintaining and regulating cellular and subcellular functions of virtually all cells. Four major roles of Zn^{2+} have been reported: 1), it binds tightly to metalloenzymes and serves as a cofactor in gene expression and enzymatic reactions (3); 2), it is abundant in the brain, where it is localized in the presynaptic terminals, is coreleased with glutamate (4,5), and regulates neuronal excitability and synaptic plasticity (6,7); 3), it is involved in many pathological neuromodulatory events, and the accumulation of Zn^{2+} during and after transient global ischemia (8,9) can also affect cardiac functions (10,11); and 4), it regulates conductivity of VDCCs (12–14) and affects Ca^{2+} signaling.

Zn^{2+} block of VDCCs has been found in various neuronal preparations from different species, including DRG neurons (12,15), hypothalamic neurons (13,16), paleocortical neurons (17), thalamic relay neurons (14), and pelvic neurons (18). The sensitivity of native calcium channels to Zn^{2+} is highly variable, with IC_{50} values ranging from 7 μM (13) to 300 μM (15). In these studies, Zn^{2+} inhibition of the VDCCs was primarily affected by the animal species used and the cell type studied (14,19). Most neurons express multiple calcium channel subtypes, and each channel has a distinct physiological role. Thus, the sensitivity of specific calcium channels to zinc inhibition, which has not yet been determined, is critically important for a better understanding of their particular role in calcium conductance.

Inhibition of different calcium channel subtypes by various inorganic and organic calcium channel blockers (20,21) has been studied in cells in which the channel subtypes were transiently expressed. High-voltage–activated (HVA) calcium channels are heteromultimers consisting of α_1, α_2, β-, and δ-subunits. The α_1 subunit, which contains the channel pore region, encompassing the selectivity filter locus, plays the predominant role in determining channel conductance. Currently, 11 VDCC α_1 subunits have been cloned, including four HVA Ca_V1 L-type channels ($Ca_V1.1/\alpha_{1S}$, $Ca_V1.2/\alpha_{1C}$, $Ca_V1.3/\alpha_{1D}$, and $Ca_V1.4/\alpha_{1F}$); three HVA Ca_V2 non-L-type calcium channels ($Ca_V2.1/\alpha_{1A}$, $Ca_V2.2/\alpha_{1B}$, and $Ca_V2.3/\alpha_{1E}$); and three low-voltage-activated (LVA) Ca_V3 T-type channels ($Ca_V3.1/\alpha_{1G}$, $Ca_V3.2/\alpha_{1H}$, and $Ca_V3.3/\alpha_{1I}$) (22–24). The electrophysiological and pharmacological properties of the α_1 subunits have been well described. For instance, α_{1C} ($Ca_V1.2$) is found in dihydropyridine-sensitive L-type channels; α_{1A} ($Ca_V2.1$) in ω-agatoxin IVA-sensitive P-/Q-type channels; α_{1B} ($Ca_V2.2$) in ω-conotoxin GVIA-sensitive N-type channels; and α_{1E} ($Ca_V2.3$) in R-type channels. T-type calcium channels contain one of three α_1 subunits, α_{1G} ($Ca_V3.1$), α_{1H} ($Ca_V3.2$), and α_{1I} ($Ca_V3.3$), and their specific pharmacological properties have not yet been clearly identified (25). In this study, we systematically determined the effect of Zn^{2+} on transiently expressed HVA and LVA calcium channels and demonstrated that sensitivity to Zn^{2+} inhibition is α_1 subtype specific and may be dependent on selectivity filter residues outside of the EEEE/EEDD locus of the channels.

Submitted December 19, 2006, and accepted for publication April 23, 2007.

Address reprint requests to Zhong-Ping Feng, Dept. of Physiology, University of Toronto, Toronto, Ontario, Canada M5S 1A8. Tel.: 416-946-5506; Fax: 416-978-4940; E-mail: zp.feng@utoronto.ca.

Editor: Eduardo Perozo.

0006-3495/07/08/1175/09 $2.00

doi: 10.1529/biophysj.106.103333

METHODS

Tissue culture and transient transfection

Human embryonic kidney tsA-201 cells were maintained in standard DMEM supplemented with 10% fetal bovine serum, 200 units/ml penicillin, and 0.2 mg/ml streptomycin at 37°C in a CO_2 incubator (26,27). Cells were split with trypsin-EDTA, plated on glass coverslips at 10% confluency, and allowed to recover for 12 h at 37°C. The cells were then transiently transfected with expression vectors containing cDNAs encoding wild-type or mutant calcium channel α_1, β_{1b}, and α_2-δ subunits and enhanced green fluorescent protein (eGFP) at a 1:1:1:0.2 molar ratio, using a standard Ca^{2+} phosphate protocol (26). All wild-type α_1 (α_{1G}, AF290212; α_{1H}, AF290213; α_{1I}, AF290214; α_{1C}, M67515; α_{1A}, M64373; α_{1B}, M92905; and α_{1E}, L15453), β_{1b}, and α_2-δ subunits cDNAs were generous gifts from Dr. Terry Snutch (University of British Columbia, Vancouver, British Columbia, Canada), and mutant α_{1B} subunit cDNAs were generous gifts from Dr. Gerald Zamponi (University of Calgary, Calgary, Alberta, Canada). After 12 h, the cell culture medium was replaced with fresh medium. The cells were allowed to recover for an additional 12 h and were subsequently kept at 28°C in 5% CO_2 for 1–2 days before physiological recordings were made.

Chemicals and solutions

All chemicals used in the cell culture were purchased from GIBCO (Invitrogen, Burlington, Canada). Chemicals used for physiological recordings were purchased from Sigma (St. Louis, MO).

Electrophysiology

Whole-cell patch-clamp (ruptured) recordings were performed using a MultiClamp 700A amplifier (Axon Instruments, Foster City, CA) linked to a personal computer equipped with pClamp9. Patch pipettes (Sutter borosilicate glass, BF 150-86-15) were pulled using a Sutter P-87 microelectrode puller and subsequently fire polished using a Narashige microforge. Pipettes (in the range of 2–4 MΩ) were filled with internal solution containing 108 mM Cs-methanesulfonate, 4 mM $MgCl_2$, 9 mM EGTA, and 9 mM HEPES (adjusted to pH 7.2 with TEA-OH). The cells were transferred to a 3.5-cm culture dish containing recording solution comprised of 20 mM $BaCl_2$ (or $CaCl_2$), 1 mM $MgCl_2$, 10 mM HEPES, 40 mM TEACl, 10 mM glucose, and 87.5 mM CsCl (adjusted to pH 7.2 with TEA-OH). Currents were elicited by stepping from a holding potential of −100 mV to various test potentials; Clampex software was used to control this process. Data were filtered at 1 kHz using a four-pole Bessel filter and digitized at a sampling frequency of 2 kHz.

Data analyses

All data were analyzed using Clampfit (Axon); curve fittings were carried out using SigmaPlot 4.0 (Jandel Scientific). Dose-response curves were fitted using the equation $I/I_0 = 1/(1 + ([Zn^{2+}]/IC_{50})^n)$, where I is the peak current response to a given test potential in the presence of Zn^{2+}, I_0 is the current obtained in the drug-free condition (the control condition), $[Zn^{2+}]$ is the zinc concentration, IC_{50} is the concentration at which 50% inhibition is obtained, and n is the Hill coefficient. Current-voltage relations obtained from peak current amplitude were fitted to the equation $I = (G_{max}(V - V_r))/(1 + \exp((V_h - V)/S))$, where I is the measured peak current, G_{max} is the slope conductance, V is the test potential, V_r is the apparent reversal potential, V_h is the potential of half-maximal activation, and S is the slope of activation.

Statistics

Statistical analyses were carried out using SigmaStat 3.0 software (SPSS, Chicago, IL). The significance of differences between mean values from each experimental group was tested using a Student's t-test for two groups and one-way analysis of variance for multiple comparisons. Differences were considered significant if $p < 0.05$.

RESULTS AND DISCUSSION

Sensitivities of calcium channels to zinc inhibition are α_1 subunit specific

Differential inhibitory effects of Zn^{2+} on LVA calcium channels

We investigated the inhibitory effect of Zn^{2+} on three recombinant low-voltage–dependent T-type calcium channels (α_{1G}, α_{1H}, and α_{1I}) using a transient expression system. We evoked whole-cell currents in tsA-201 cells transiently expressing T-type calcium channels by a 10-ms depolarization step of −20 mV from a holding potential of −100 mV in 20 mM Ba^{2+}. Representative current recordings for cells expressing $Ca_V3.2$ (α_{1H}) obtained for various Zn^{2+} concentrations are shown in Fig. 1 *A1*, and the corresponding time course of the development of the Zn^{2+} inhibition on the tail current is shown in Fig. 1 *A2*. Inhibition of the current was observed within 10 s of exposing cells to Zn^{2+} and rapidly reached equilibrium. Inhibition of the T-type calcium channel was reversible, as rapid recovery from Zn^{2+} inhibition was nearly complete after washout and removal of the Zn^{2+}, consistent with previous reports for native neurons (14,19). Fig. 1 *B* shows a mean concentration-response curve fitted to the Hill equation (with a Hill coefficient of ~1). As determined from eight independent experiments, the mean IC_{50} value of Zn^{2+} for the $Ca_V3.2$ channel was 24.1 ± 1.9 μM.

The inhibitory effect of Zn^{2+} on $Ca_V3.1$ (α_{1G}) and $Ca_V3.3$ (α_{1I}) channels was determined using the same protocol as was used for the $Ca_V3.2$ channels (α_{1H}). Interestingly, these channels exhibited a different sensitivity to Zn^{2+}, as the mean IC_{50} values for Zn^{2+} varied depending on the α_1 subunit contained in the channel. Fig. 1 *B* shows a comparison of the mean concentration-response curves of $Ca_V3.2$ (α_{1H}) and $Ca_V3.3$ (α_{1I}) channels to the response curves for $Ca_V3.1$ (α_{1G}) channels. The mean concentration-response curve of the $Ca_V3.2$ channel shifted to a lower concentration than the response curves of the $Ca_V3.1$ or $Ca_V3.3$ channels (Fig. 1 *B*), indicating that the $Ca_V3.2$ channels are more sensitive to Zn^{2+} inhibition than are the other T-type calcium channels. The mean IC_{50} values of Zn^{2+} for the three LVA channels are compared in Fig. 1 *C*. The IC_{50} of Zn^{2+} for the $Ca_V3.2$ (α_{1H}) channels (24.1 ± 1.9 μM, $n = 8$) was significantly lower than that of the $Ca_V3.1$ (α_{1G}) (196.5 ± 50.4 μM, $n = 7$; $p < 0.05$) and $Ca_V3.3$ (α_{1I}) channel (152.2 ± 30.6 μM, $n = 8$; $p < 0.05$). The Hill coefficient for $Ca_V3.2$ (α_{1H}) was 1.3 ± 0.2, that for $Ca_V3.2$ (α_{1G}) was 1.1 ± 0.1, and the one for $Ca_V3.3$ (α_{1I}) was 1.0 ± 0.1. The differences of the Hill coefficients among three T-type channels were not statistically significant ($p > 0.05$), consistent with a recent report (28). These results demonstrate that the sensitivity to Zn^{2+} of the LVA calcium

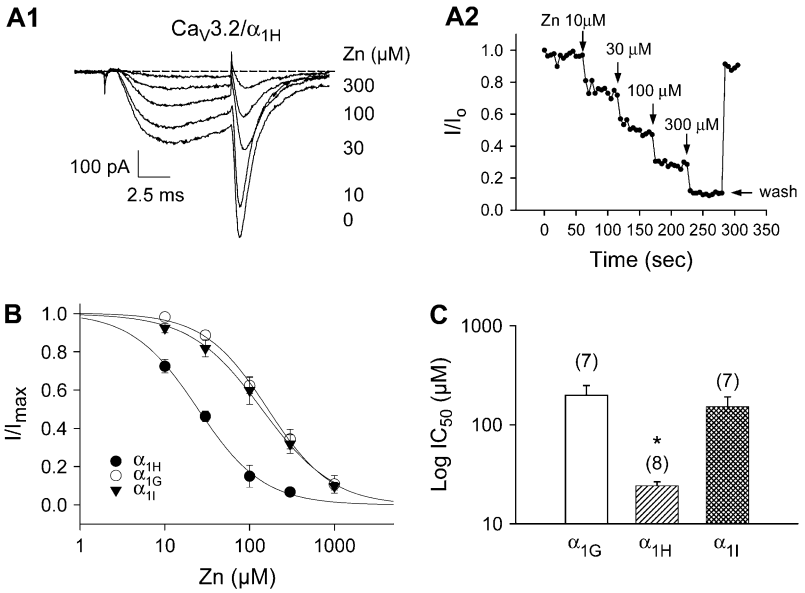

FIGURE 1 Differential block effect of Zn^{2+} on LVA calcium channels. (*A*) A typical representative of the dose-dependent blockade effect of Zn^{2+} on whole-cell current of $Ca_V3.2$ (α_{1H}) calcium channels. (*A1*) Current traces recorded in 20 mM Ba^{2+} for $Ca_V3.2$ channels during 10-ms voltage steps from a holding potential of −100 mV to −20 mV in the absence or presence of various Zn^{2+} concentrations, as indicated. Note that the current amplitude decreased with an increase in Zn^{2+} concentrations. (*A2*) The corresponding time course of development of block and recovery from Zn block in $Ca_V3.2$ channels is shown in *A1*. Comparison of the average dose-response curves (*B*) and IC_{50} values (*C*) of Zn^{2+} block effect on three LVA calcium channels. The cells have been recorded from: $Ca_V3.1$ (α_{1G}), $n = 7$; $Ca_V3.2$ (α_{1H}), $n = 8$; and $Ca_V3.3$ (α_{1I}), $n = 7$. The data are presented as mean ± SE. (*) Statistical significance ($p < 0.05$) among the groups. The number in the parentheses in *C* indicates the number of cells used for the recordings.

channels is intrinsically different among the subtypes, with $Ca_V3.2$-type channels being the most sensitive to the inhibitory effects of Zn^{2+}. These findings are consistent with previous reports that α_{1H} has a higher sensitivity to Zn^{2+} than α_{1G} and α_{1I} (18,28). The Hill coefficients of Zn^{2+} for T-type channels varied ~1, indicating a single binding site or no cooperative interaction between Zn^{2+} binding sites under the Ba^{2+} condition. The change in the potency of Zn^{2+} among the LVA channels likely results from the different binding affinities, assuming that Zn^{2+} binds to a similar site. Because the selectivity filter of all T-type channels has a conserved EEDD motif (29–31), the differing sensitivities, reflected by IC_{50} values, of the T-type channels indicate that the Zn^{2+} inhibitory effect on these channels is likely regulated by the residues outside of the pore EEDD motif.

Differential inhibitory effects of Zn^{2+} on HVA calcium channels

We next performed whole-cell current recordings to determine the effect of Zn^{2+} on recombinant high- and intermediate-voltage–dependent calcium channels transiently expressed in tsA-201 cells. Similar to the results obtained for the LVA calcium channels, we found that Zn^{2+} inhibited the HVA calcium channels in a concentration-dependent manner (Fig. 2). Representative Ba^{2+} current recordings obtained for the L-type calcium channels ($\alpha_{1C} + \beta_{1b} + \alpha_2 - \delta$) in various concentrations of Zn^{2+} are shown in Fig. 2 *A*, and the corresponding time course of the development for Zn^{2+} inhibition is shown in Fig. 2 *B*. We evoked currents by using a depolarization step of +10 mV from a holding potential of −100 mV in 20 mM Ba^{2+}. Inhibition of the current developed within 10 s of exposure to Zn^{2+}, rapidly reached equilibrium, and was eliminated promptly after washout of the Zn^{2+} (Fig. 2 *A2*), similar to the results obtained in experiments using transiently expressed T-type calcium channels (Fig. 1 *B*). Fig. 2 *B* shows the mean concentration-response curve fitted using the Hill equation (with a Hill coefficient of ~1). As determined from eight independent experiments, the mean IC_{50} value of Zn^{2+} inhibition of the L-type channel was 10.9 ± 3.4 μM.

The inhibitory effects of Zn^{2+} on N- (α_{1B}), P/Q- (α_{1A}), and R-type (α_{1E}) calcium channels (coexpressed with β_{1b} and $\alpha_2 - \delta$ subunits) were determined using the same protocol used to determine the effect for L-type calcium channels (α_{1C}). Similar to T-type channels, HVA calcium channels responded differentially to the inhibitory effect of zinc, as the mean IC_{50} values varied depending on the α_1 subunit. As depicted in the concentration-response curves in Fig. 2 *B*, the mean concentration-response curves for N- (α_{1B}), P/Q- (α_{1A}), and R-type (α_{1E}) calcium channels were shifted to higher concentrations compared to the response curve for the L-type calcium channel (Fig. 2 *B*), indicating that these channels are less sensitive to Zn^{2+} inhibition than is the L-type calcium channel. The IC_{50} values of all four HVA calcium channels are compared in Fig. 2 *C*. The Zn^{2+} IC_{50} value for the N-type (98.0 ± 17.9 μM, $n = 12$) and P/Q-type (110.0 ± 7.0 μM, $n = 8$) channels are ~10-fold greater than that of the L-type (10.9 ± 3.4 μM, $n = 8$) channel. These differences are statistically significant ($p < 0.05$, Fig. 2 *C*). The Zn^{2+} IC_{50} value for the R-type calcium channel was 31.8 ± 12.3 μM ($n = 8$), which is significantly higher than that of the L-type channel ($p < 0.05$) but lower than that of N- and P-/Q-type channels ($p < 0.05$). These results clearly demonstrate that the sensitivity to the Zn^{2+} inhibitory effect of the HVA calcium channels differs intrinsically with the highest sensitivity found in the L-type channels and the lowest sensitivity in the N- and P/Q- type channels. Again, as

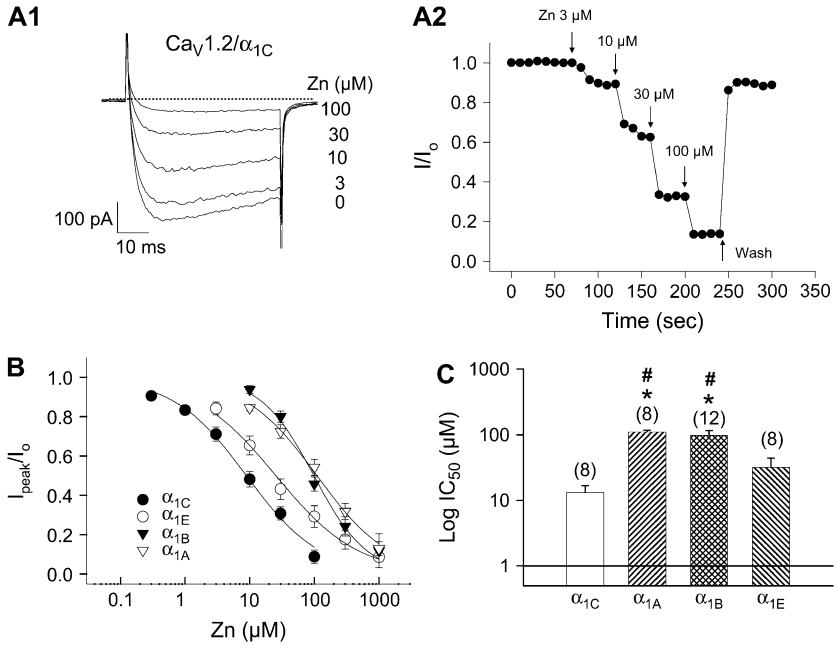

FIGURE 2 Differential block effect of Zn^{2+} on HVA calcium channels. (*A*) A typical representative of the dose-dependent blockade effect of Zn^{2+} on whole-cell current of $Ca_V1.2$ (α_{1C}) calcium channels. (*A1*) Current traces recorded in 20 mM Ba^{2+} for $Ca_V1.2$ channels during 10-ms voltage steps from a holding potential of −100 mV to −20 mV in the absence or presence of various Zn^{2+} concentrations, as indicated. Note that the current amplitude decreased with an increase in Zn^{2+} concentrations. (*A2*) The corresponding time course of development of block and recovery from Zn block in $Ca_V1.2$ channels is shown in *A1*. Comparison of the average dose-response curves (*B*) and IC_{50} values (*C*) of Zn^{2+} block effect on four HVA calcium channels. The Hill coefficients to Zn^{2+} were $Ca_V1.2$ (α_{1C}), 0.88 ± 0.08 ($n = 8$); $Ca_V2.1$ (α_{1A}), 0.91 ± 0.06 ($n = 8$); $Ca_V2.2$ (α_{1B}), 0.92 ± 0.13 ($n = 12$); and $Ca_V2.3$ (α_{1E}), 0.55 ± 0.05 ($n = 8$). The data are presented as mean ± SE. Statistical significance ($p < 0.05$) (*) to $Ca_V1.2$ (α_{1C}) and (#) to $Ca_V2.3$ (α_{1E}) when one-way analysis of variance was used for comparison. The number in the parentheses in *C* indicates the number of cells used for the recordings.

seen in LVA calcium channels, the Zn^{2+} effect on HVA calcium channels varied depending on the channel α_1 subtype, and this variation in sensitivity did not seem directly related to the selectivity filter EEEE residues, which are conserved in all HVA calcium channels (32,33).

Zn^{2+} block and the selectivity filter of calcium channels

The selectivity filter of the pore region of T-type channels has an EEDD locus (29–31), whereas the selectivity filter in high-voltage–gated channels has an EEEE locus (32,33). We found that the variation in sensitivity to Zn^{2+} block of the channels was independent of these conserved selectivity filter residues. Based on the observed Zn^{2+} IC_{50} values for the various channels, we found that the order of sensitivity to the block by Zn^{2+} was approximately $\alpha_{1C} > \alpha_{1H} > \alpha_{1E} > \alpha_{1B} = \alpha_{1A} > \alpha_{1I} = \alpha_{1G}$ when Ba^{2+} was used as the charge carrier.

Most HVA calcium channels conduct Ba^{2+} ~2-fold better than they conduct Ca^{2+} (see McDonald et al. (34)). This difference seems to result from a higher binding affinity for Ca^{2+} ions than for Ba^{2+} ions at the EEEE locus of the channel pore region (26,32,33,35). In contrast, the Ca^{2+} conductance of the LVA channels is similar to or slightly greater than that of Ba^{2+} (36–38). If Zn^{2+} inhibition of these channels depends on the charge carrier species and hence on the properties of the permeation pathway lining the pore region, the sensitivity of the HVA calcium channels to Zn^{2+} would be expected to be less in Ca^{2+} than in Ba^{2+}, whereas that of T-type channels would remain unchanged. Therefore, we tested whether Zn^{2+} inhibition of these channels is affected by the charge carrier. Specifically, $Ca_V2.2$ N-type and $Ca_V3.1$ T-type calcium channels were compared because their IC_{50} values in 20 mM Ba^{2+} were similar (100–200 μM), when the inhibitory effect of Zn^{2+} on Ba^{2+} and Ca^{2+} currents was measured. Fig. 3 *A* shows the *I-V* curves for both channels in Ba^{2+} (Fig. 3, *A1* and *A3*) and Ca^{2+} (Fig. 3, *A2* and *A4*) with or without 100 μM Zn^{2+}. Consistent with previous reports (26,37–39), the current amplitude ratio between Ba^{2+} and Ca^{2+} (I_{Ba}/I_{Ca}) was ~2 for the N-type channel and ~0.8 for the $Ca_V3.1$ channel (Fig. 3, *inset*), and the *I-V* relations of the channels were not affected by Zn^{2+}. As shown in Fig. 3 *B*, the IC_{50} for $Ca_V2.2$ α_{1B} significantly increased (by ~14-fold, $p < 0.05$) in 20 mM Ca^{2+} (1.21 ± 0.08 mM, $n = 8$) as compared to that in 20 mM Ba^{2+} (98.0 ± 17.9 μM, $n = 12$), suggesting that the current carrier species plays a role in regulating Zn^{2+} inhibition of the N-type channel. In contrast, the T-type $Ca_V3.1$ (α_{1G}) channel had a similar sensitivity to Zn^{2+} in Ba^{2+} (IC_{50} 198.5 ± 50.4 μM, $n = 7$) and in Ca^{2+} (IC_{50} 132.8 ± 21.2 μM, $n = 7$, consistent with Jeong et al. (18)); and the difference in the IC_{50} values was not statistically significant ($p > 0.05$).

Multiple mechanisms of Zn^{2+} block of VDCCs have been suggested, including pore block, surface charge screening, and gating modification (14,19,40); however, these mechanisms vary among the different channel subtypes. Our findings show that the charge carrier–dependent Zn^{2+} sensitivity cannot be explained by either hydration energy or surface charge screening alone. Experimental hydration energies for Ba^{2+}, Ca^{2+}, and Zn^{2+} are 298, 360, and 467 kcal/mol (41,42), respectively. If ion access to the pore required complete removal of the hydration shells, then these energies indicate that permeation/block follows the order $Ba^{2+} > Ca^{2+} > Zn^{2+}$. Thus, Zn^{2+} block would be expected to be more sensitive to Ba^{2+} than to Ca^{2+}. Although this seems to be the case for the $Ca_V2.2$ (α_{1B}) channel, it does not explain

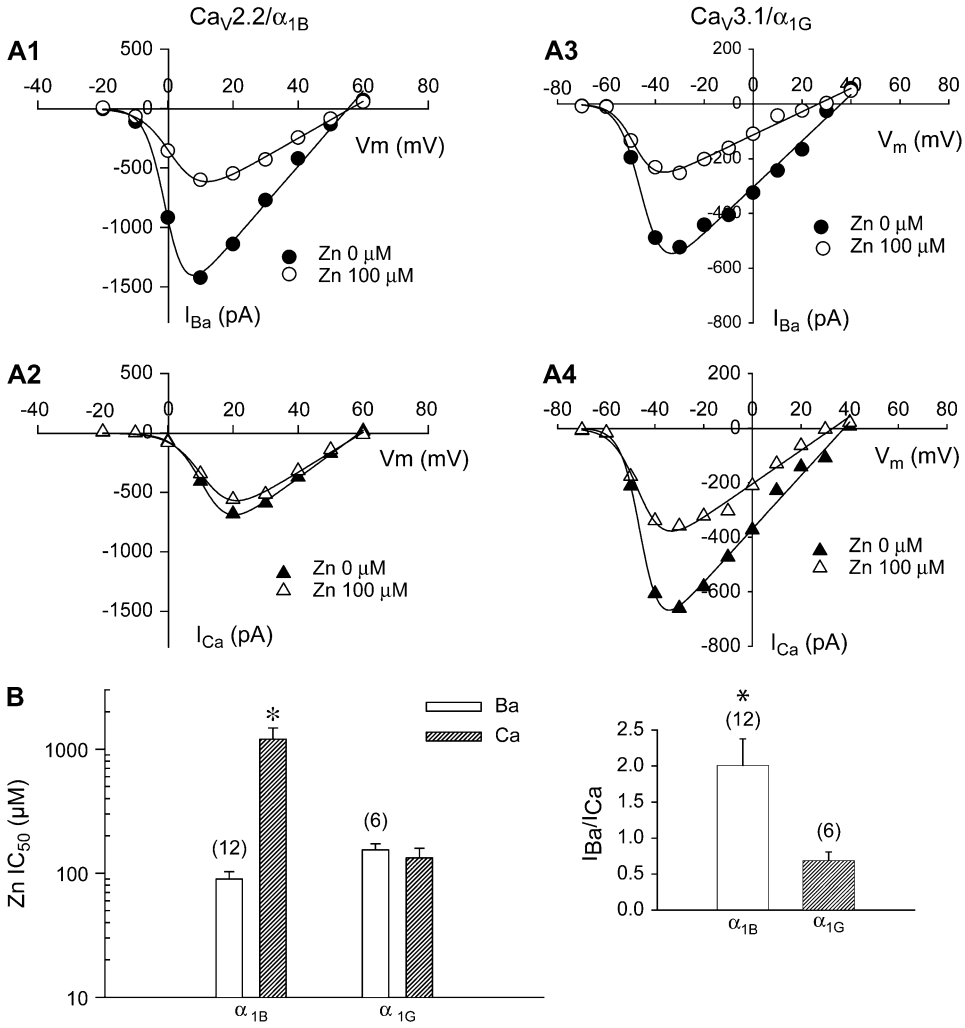

FIGURE 3 Comparison of Zn effects on I_{Ca} and I_{Ba} of $Ca_V2.2$ (α_{1B}) N-type and $Ca_V3.1$ (α_{1G}) T-type calcium channels. (*A*) Representative current-voltage curves of $Ca_V2.2$ (α_{1B}) N-type and $Ca_V3.1$ (α_{1G}) T-type calcium channels in the absence or presence of 100 μM Zn^{2+}: $Ca_V2.2$ (α_{1B}) channels (*A1*); 20 mM Ba^{2+} (*A2*); 20 mM Ca^{2+}. $Ca_V3.1$ (α_{1G}) channels: (*A3*) 20 mM Ba^{2+}; (*A4*) 20 mM Ca^{2+}. (*Inset*) Comparison of the peak Ba^{2+} to Ca^{2+} current ratio of $Ca_V2.2$ (α_{1B}) and $Ca_V3.1$ (α_{1G}) calcium channels. (*B*) Summary of IC_{50} values of Zn^{2+} on $Ca_V2.2$ (α_{1B}) and $Ca_V3.1$ (α_{1G}) channels. The blockade effects of Zn^{2+} on $Ca_V2.2$ (α_{1B}) channels are ~10-fold higher in Ca^{2+} than in Ba^{2+} conditions, whereas those on $Ca_V3.1$ (α_{1G}) channels are similar. The data are presented as mean ± SE. from 12 cells expressing $Ca_V2.2$ (α_{1B}) channels and 6 cells expressing $Ca_V3.1$ (α_{1G}) channels. (*) Statistical significance ($p < 0.05$) between the different conditions. The number in parentheses indicates the number of cells used for the recordings.

the differences seen in all the channels. For instance, all three T-type channels have similar Ba^{2+} to Ca^{2+} current ratios, ~0.8, and the differences in Zn^{2+} sensitivities in the presence of Ca^{2+} and Ba^{2+} conditions are inconsistent. α_{1I} sensitivity was substantially higher in Ba^{2+} (IC_{50} 152 μM; Fig. 1 *D*) than reported in Ca^{2+} (IC_{50} 470 μM (18)); α_{1H} was lower in Ba^{2+} (IC_{50} ~ 24 μM; Fig. 1 *D*) than in Ca^{2+} (IC_{50} 2.4 μM (18)); and in this study we showed that Zn^{2+} sensitivity of $Ca_V3.1$ (α_{1G}) was similar in Ba^{2+} and Ca^{2+} (Fig. 3). Surface charge screening also does not explain the differences in the Zn^{2+} effect between the subtypes. Mg^{2+} and Zn^{2+} are identically charged and contribute to surface charge screening equally. Mg^{2+} preferentially blocks Ba^{2+} currents more than Ca^{2+} currents through α_{1G} (43), whereas we showed that Zn^{2+} block of α_{1G} was comparable in Ba^{2+} and Ca^{2+}. Thus, neither hydration energy nor surface charge screening alone appears to explain the influence of ion species–dependent modulation of channel conductance and Zn^{2+} block.

The selectivity filter of VDCCs alone does not explain the differences in the ion-dependent Zn^{2+} block effect. The molecular determinants of ion selectivity in VDCCs resides on the selectivity filter loci encoding EEEE/EEDD motif; however, α_{1E} encoded with EEEE locus seen in HVA channels, as an exception, exhibits a higher permeability to Ca^{2+} than to Ba^{2+}, similar to LVA channels (38). Thus, additional residues other than the EEEE/EEDD motif are involved in ion selectivity of the pore. Previous studies in K^+ (44) and Na^+ (45) channels demonstrated that metal binding sites are dependent on the unique residues near the selectivity filter. Mutation of these residues substantially affected Zn^{2+} block. These findings bring into question whether Ca^{2+} channels may also contain specific extrapore sites regulating Zn^{2+} block.

Zn^{2+} blockade is regulated by the putative EF-hand extrapore region of N-type calcium channel

We previously reported that ion permeation in N-type channels is modulated by a putative EF-hand motif located in domain III near the EEEE locus (26). It contains a central glycine residue flanked by three acidic residues, reminiscent of the classical EF-hands of Ca^{2+} binding proteins (46,47).

Disruption of this motif reduces the ability of the channel to distinguish between Ba^{2+} and Ca^{2+} ions without affecting the pore function. To determine whether this putative EF-hand motif is also involved in regulating Zn^{2+} inhibition of these channels, we compared the IC_{50} values of Zn^{2+} obtained for wild-type N-type calcium channels to those obtained for two EF-hand mutant channels: a triple mutant in which all three negative charge residues in the putative EF-hand structure are replaced with positively charged residues (E1321K, D1323R, E1332R), and the G1326P mutant in which the central glycine is replaced with a proline. The latter mutant alters the ion permeability of the N-type channel by disrupting the EF-hand structure without changing the net local surface charge (26). We previously showed that these mutant channels exhibit biophysical properties similar to those of the wild-type channel (26). Representative recordings shown in Fig. 4 *A* reveal that Zn^{2+} inhibited the current activity of each mutant for both carriers, Ba^{2+} and Ca^{2+}, in a dose-dependent manner. The mean Zn^{2+} IC_{50} values were comparable between the wild-type (98.0 ± 17.9 μM, $n = 12$) and mutant channels in 20 mM Ba^{2+} (triple, 79.2 ± 13.9 μM, $n = 8$; G1326P, 60.0 ± 5.5 μM, $n = 11$); however, the mean Zn^{2+} IC_{50} was significantly ($p < 0.05$) reduced in the mutant channels (wt, 1210 ± 80 μM, $n = 8$; triple, 290 ± 50 μM, $n = 8$; G1326P, 350 ± 70 μM, $n = 11$) when Ca^{2+} was used as the charge carrier (Fig. 4 *B*). Both the neutralization of three negatively charged residues and the replacement of central glycine with proline in the putative EF-hand region caused a similar effect on the Zn^{2+} sensitivity in Ca^{2+} condition, indicating that the effect is most likely independent of local surface charge screening. These results suggest that the putative EF-hand motif is involved in regulating Zn^{2+} block effect.

The putative EF-hand in the domain III H5 loop of the N-type calcium channel α_{1B} subunit forms a helix-coil-helix structure (48). A molecular structure model suggests that it is capable of interacting with Ca^{2+}, although its sequence exhibits some variation compared to the classical EF-hand. The putative EF-hand was previously shown to be involved in Ba^{2+} and Ca^{2+} permeability of N-type channels (26) as well as ω-conotoxin GVIA block (49). Eight of the HVA Ca^{2+} channel α_1 subunits appear to have this putative EF-hand motif (26), but none of the LVA Ca^{2+} channels, Na^+ channels, and K^+ channels have it in the homologous region (Fig. 5). Because mutation of the EF-hand motif of N-type channels increased Zn^{2+} sensitivity in Ca^{2+} toward that seen

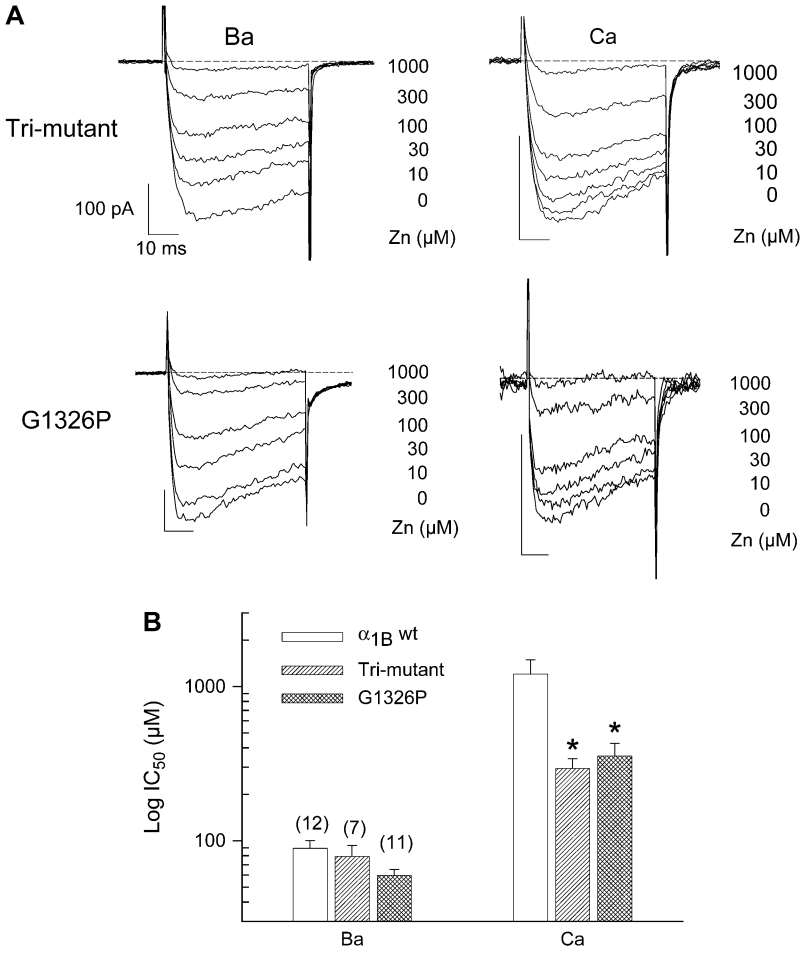

FIGURE 4 Mutations of the putative EF-hand in domain III of the $Ca_V2.2$ (α_{1B}) N-type channel affected Zn^{2+} sensitivity. (*A*) Representative current traces from two mutants of $Ca_V2.2$ (α_{1B}) N-type calcium channels (trimutant, and G1326P) in the absence or presence of various concentrations of Zn^{2+}, as indicated, in either 20 mM Ba^{2+} or 20 mM Ca^{2+}. Trimutant: E1321K, D1323R, E1332R. (*B*) Summary of IC_{50} values of Zn^{2+} on the wild-type and mutant $Ca_V2.2$ (α_{1B}) calcium channels. The data are presented as mean ± SE. (*) Statistical significance ($p < 0.05$) between the wild-type and mutant channels under the same recording conditions. The number in the parentheses indicates the number of cells used for the recordings.

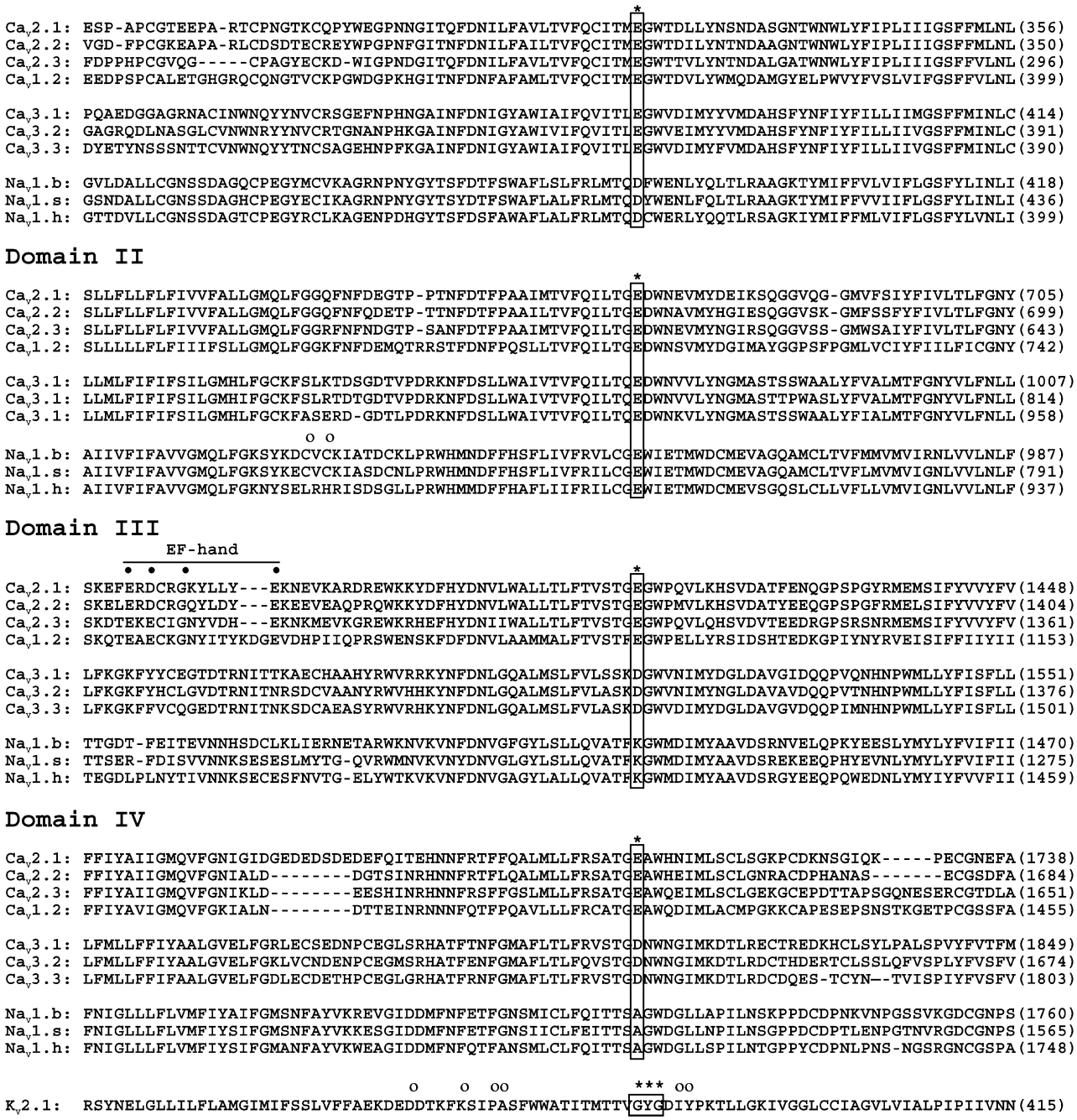

FIGURE 5 Protein sequence alignments showing the extended pore regions of representative voltage-dependent calcium channels, sodium channels, and potassium channel. The box and asterisks indicate the identified selectivity filter residues. The solid line indicates the putative EF-hand motif region; solid circle, the conserved acidic residues and the central glycine; open circle, critical sites affecting Zn sensitivity of the channels. b, brain; s, skeletal muscle; and h, heart.

in α_{1G} T-type channels, it may be involved in distinguishing between Zn^{2+} block of the HVA and LVA channels. In the typical EF-hand motif, the $-Z$ position glutamic acid residue contributes two carboxylate oxygen atoms to coordinate a Ca^{2+}, and the central glycine is located at sharp bend position critical for Ca^{2+} coordination (46,47). Shown in Fig. 5, both $-Z$ acidic residue ($Ca_V2.1$, E1376; $Ca_V2.2$, E1332; $Ca_V2.3$, E1289; $Ca_V1.2$, E1081) and the central glycine ($Ca_V2.1$, E1370; $Ca_V2.2$, E1326; $Ca_V2.3$, E1283; $Ca_V1.2$, E1072) are conserved among four HVA Ca^{2+} channels; however, the remaining residues vary among the channels. In comparison to the Ca_V2 α_1 subunits, $Ca_V1.2/\alpha_{1C}$ contains three additional residues, K1078, D1079, and G1080, between the central glycine (G1072) and the $-Z$

glutamic acid (E1081), which may weaken the effectiveness of the putative EF-hand motif in coordinating Ca^{2+}. This could explain our finding that Zn^{2+} sensitivity of $Ca_V1.2/\alpha_{1C}$ is higher than that of the Ca_V2 channels. Taken together, the presence and composition of the putative EF-hand motif may be partly responsible for the differences in Zn^{2+} block between HVA channels and LVA channels as well as between the HVA channels.

The differences in Zn^{2+} block effects on LVA channels do not appear to be explained by the putative EF-hand motif because it is absent in their α_1 subunit. In this study, we found that under Ba^{2+} conditions α_{1H} was ~10-fold more sensitive to Zn^{2+} than α_{1G} and α_{1I}. In comparison, under Ca^{2+} conditions, α_{1H} was ~100- to 200-fold more sensitive to Zn^{2+} than α_{1G} and α_{1I} (18,28). These charge carrier-dependent differences in Zn^{2+} sensitivities indicate that block is modulated by residues outside the EEDD selectivity filter locus. Similarly, α_{1H} has been shown to have higher sensitivities to Cu^{2+} and Ni^{2+} than the other T-type channels (18) through a mechanism that may involve noncharged residues. Cysteine or histidine pairs are known to be able to coordinate divalent ions and have been shown to affect ion selectivity when found in the pore regions of Na^+ (45) and K^+ channels (44). A recent report showed that the point mutation H191Q in the S3-S4 loop of domain I reduced Ni^+ block of α_{1H} (50), indicating that H191 is critical for Ni^+ block. Whether the high-sensitivity block of α_{1H} by Zn^{2+} also resides with this residue remains to be tested, but the study lends further support to the notion that extrapore residues can affect ion block of VDCCs.

In conclusion, we have systematically tested and compared the Zn^{2+} sensitivities of HVA and LVA calcium channels in a transient expression system. We show that Zn^{2+} block of VDCCs is dependent on the pore-forming α_1 subunit, but variation in the Zn^{2+} sensitivities of the channel subtypes is independent of EEEE/EEDD locus and is differentially regulated by permeant ions. Zn^{2+} block of the $Ca_V2.2/\alpha_{1B}$ N-type channel is modulated via a putative EF-hand motif outside of the EEEE locus. Although it is not clear how the EF-hand is involved in modulation of Zn^{2+} block, we envision a model in which Zn^{2+} binds at the pore of the channel, and other regions, such as the EF-hand, modulate the interaction between Zn^{2+} and the pore. Our study supports the notion that multiple mechanisms are involved in the channel subtype-dependent Zn^{2+} block. Further studies are required to identify other molecular determinants underlying the differences in the block effect of Zn^{2+} on the various calcium channel subtypes and to elucidate the mechanisms involving these determinants.

We thank Dr. Terry Snutch and Dr. Gerald Zamponi for the calcium channel constructs. We thank Clinton Doaring for his technical assistance.

This work was supported by an operating grant to Z.P.F. from the Heart and Stroke Foundation of Ontario (grant No. NA 5302), startup funds from the Dept. of Physiology, the Faculty of Medicine, and the University of Toronto, and equipment grants from the Canada Foundation for Innovation and the Ontario Innovation Trust. Z.P.F. holds a New Investigator Award from the Canadian Institutes of Health Research and a Premier's Research Excellence Award of Ontario.

REFERENCES

1. Catterall, W. A. 2000. Structure and regulation of voltage-gated Ca^{2+} channels. *Annu. Rev. Cell Dev. Biol.* 16:521–555.
2. Reuter, H., S. Kokubun, and B. Prod'hom. 1986. Properties and modulation of cardiac calcium channels. *J. Exp. Biol.* 124:191–201.
3. Takeda, A., A. Minami, Y. Seki, and N. Oku. 2004. Differential effects of zinc on glutamatergic and GABAergic neurotransmitter systems in the hippocampus. *J. Neurosci. Res.* 75:225–229.
4. Assaf, S. Y., and S. H. Chung. 1984. Release of endogenous Zn^{2+} from brain tissue during activity. *Nature.* 308:734–736.
5. Frederickson, C. J., L. J. Giblin III, B. Rengarajan, R. Masalha, C. J. Frederickson, Y. Zeng, E. V. Lopez, J. Y. Koh, U. Chorin, L. Besser, M. Hershfinkel, Y. Li, R. B. Thompson, and A. Krezel. 2006. Synaptic release of zinc from brain slices: factors governing release, imaging, and accurate calculation of concentration. *J. Neurosci. Methods.* 154:19–29.
6. Smart, T. G., X. Xie, and B. J. Krishek. 1994. Modulation of inhibitory and excitatory amino acid receptor ion channels by zinc. *Prog. Neurobiol.* 42:393–441.
7. Lin, D. D., A. S. Cohen, and D. A. Coulter. 2001. Zinc-induced augmentation of excitatory synaptic currents and glutamate receptor responses in hippocampal CA3 neurons. *J. Neurophysiol.* 85:1185–1196.
8. Koh, J. Y., S. W. Suh, B. J. Gwag, Y. Y. He, C. Y. Hsu, and D. W. Choi. 1996. The role of zinc in selective neuronal death after transient global cerebral ischemia. *Science.* 272:1013–1016.
9. Turan, B., H. Fliss, and M. Desilets. 1997. Oxidants increase intracellular free Zn^{2+} concentration in rabbit ventricular myocytes. *Am. J. Physiol.* 272:H2095–H2106.
10. Bagate, K., J. J. Meiring, M. E. Gerlofs-Nijland, F. R. Cassee, H. Wiegand, A. Osornio-Vargas, and P. J. Borm. 2006. Ambient particulate matter affects cardiac recovery in a Langendorff ischemia model. *Inhal. Toxicol.* 18:633–643.
11. Graff, D. W., W. E. Cascio, J. A. Brackhan, and R. B. Devlin. 2004. Metal particulate matter components affect gene expression and beat frequency of neonatal rat ventricular myocytes. *Environ. Health Perspect.* 112:792–798.
12. Busselberg, D., B. Platt, D. Michael, D. O. Carpenter, and H. L. Haas. 1994. Mammalian voltage-activated calcium channel currents are blocked by Pb^{2+}, Zn^{2+}, and Al^{3+}. *J. Neurophysiol.* 71:1491–1497.
13. Easaw, J. C., B. S. Jassar, K. H. Harris, and J. H. Jhamandas. 1999. Zinc modulation of ionic currents in the horizontal limb of the diagonal band of Broca. *Neuroscience.* 94:785–795.
14. Noh, J. H., and J. M. Chung. 2003. Zinc reduces low-threshold Ca^{2+} currents of rat thalamic relay neurons. *Neurosci. Res.* 47:261–265.
15. Nam, S. C., and P. E. Hockberger. 1992. Divalent ions released from stainless steel hypodermic needles reduce neuronal calcium currents. *Pflugers Arch.* 420:106–108.
16. Muller, T. H., U. Misgeld, and D. Swandulla. 1992. Ionic currents in cultured rat hypothalamic neurones. *J. Physiol.* 450:341–362.
17. Malaiyandi, L. M., K. E. Dineley, and I. J. Reynolds. 2004. Divergent consequences arise from metallothionein overexpression in astrocytes: zinc buffering and oxidant-induced zinc release. *Glia.* 45:346–353.
18. Jeong, S. W., B. G. Park, J. Y. Park, J. W. Lee, and J. H. Lee. 2003. Divalent metals differentially block cloned T-type calcium channels. *Neuroreport.* 14:1537–1540.
19. Magistretti, J., L. Castelli, V. Taglietti, and F. Tanzi. 2003. Dual effect of Zn^{2+} on multiple types of voltage-dependent Ca^{2+} currents in rat palaeocortical neurons. *Neuroscience.* 117:249–264.

20. Beedle, A. M., J. Hamid, and G. W. Zamponi. 2002. Inhibition of transiently expressed low- and high-voltage-activated calcium channels by trivalent metal cations. *J. Membr. Biol.* 187:225–238.

21. Santi, C. M., F. S. Cayabyab, K. G. Sutton, J. E. McRory, J. Mezeyova, K. S. Hamming, D. Parker, A. Stea, and T. P. Snutch. 2002. Differential inhibition of T-type calcium channels by neuroleptics. *J. Neurosci.* 22:396–403.

22. Stea, A., T. W. Soong, and T. P. Snutch. 1995. Voltage-gated calcium channels. *In* Ligand- and Voltage-Gated Ion Channels. R.A.North, editor. CRC Press, Boca Raton, FL. 113–141.

23. Birnbaumer, L., K. P. Campbell, W. A. Catterall, M. M. Harpold, F. Hofmann, W. A. Horne, Y. Mori, A. Schwartz, T. P. Snutch, T. Tanabe, et al. 1994. The naming of voltage-gated calcium channels. *Neuron.* 13:505–506.

24. Ertel, E. A., K. P. Campbell, M. M. Harpold, F. Hofmann, Y. Mori, E. Perez-Reyes, A. Schwartz, T. P. Snutch, T. Tanabe, L. Birnbaumer, R. W. Tsien, and W. A. Catterall. 2000. Nomenclature of voltage-gated calcium channels. *Neuron.* 25:533–535.

25. McGivern, J. G. 2006. Pharmacology and drug discovery for T-type calcium channels. *CNS Neurol. Disord. Drug Targets.* 5:587–603.

26. Feng, Z. P., J. Hamid, C. Doering, S. E. Jarvis, G. M. Bosey, E. Bourinet, T. P. Snutch, and G. W. Zamponi. 2001. Amino acid residues outside of the pore region contribute to N-type calcium channel permeation. *J. Biol. Chem.* 276:5726–5730.

27. Hui, K., P. Gardzinski, H. S. Sun, P. H. Backx, and Z. P. Feng. 2005. Permeable ions differentially affect gating kinetics and unitary conductance of L-type calcium channels. *Biochem. Biophys. Res. Commun.* 338:783–792.

28. Traboulsie, A., J. Chemin, M. Chevalier, J. F. Quignard, J. Nargeot, and P. Lory. 2007. Subunit-specific modulation of T-type calcium channels by zinc. *J. Physiol.* 578:159–171.

29. Cribbs, L. L., J. H. Lee, J. Yang, J. Satin, Y. Zhang, A. Daud, J. Barclay, M. P. Williamson, M. Fox, M. Rees, and E. Perez-Reyes. 1998. Cloning and characterization of alpha1H from human heart, a member of the T-type Ca^{2+} channel gene family. *Circ. Res.* 83: 103–109.

30. Perez-Reyes, E., L. L. Cribbs, A. Daud, A. E. Lacerda, J. Barclay, M. P. Williamson, M. Fox, M. Rees, and J. H. Lee. 1998. Molecular characterization of a neuronal low-voltage-activated T-type calcium channel. *Nature.* 391:896–900.

31. Lee, J. H., A. N. Daud, L. L. Cribbs, A. E. Lacerda, A. Pereverzev, U. Klockner, T. Schneider, and E. Perez-Reyes. 1999. Cloning and expression of a novel member of the low voltage-activated T-type calcium channel family. *J. Neurosci.* 19:1912–1921.

32. Hess, P., and R. W. Tsien. 1984. Mechanism of ion permeation through calcium channels. *Nature.* 309:453–456.

33. Heinemann, S. H., H. Terlau, W. Stuhmer, K. Imoto, and S. Numa. 1992. Calcium channel characteristics conferred on the sodium channel by single mutations. *Nature.* 356:441–443.

34. McDonald, T. F., S. Pelzer, W. Trautwein, and D. J. Pelzer. 1994. Regulation and modulation of calcium channels in cardiac, skeletal, and smooth muscle cells. *Physiol. Rev.* 74:365–507.

35. Yue, D. T., and E. Marban. 1990. Permeation in the dihydropyridine-sensitive calcium channel. Multi-ion occupancy but no anomalous mole-fraction effect between Ba^{2+} and Ca^{2+}. *J. Gen. Physiol.* 95:911–939.

36. Nilius, B., P. Hess, J. B. Lansman, and R. W. Tsien. 1985. A novel type of cardiac calcium channel in ventricular cells. *Nature.* 316: 443–446.

37. Carbone, E., and H. D. Lux. 1984. A low voltage-activated, fully inactivating Ca channel in vertebrate sensory neurones. *Nature.* 310: 501–502.

38. Bourinet, E., G. W. Zamponi, A. Stea, T. W. Soong, B. A. Lewis, L. P. Jones, D. T. Yue, and T. P. Snutch. 1996. The alpha 1E calcium channel exhibits permeation properties similar to low-voltage-activated calcium channels. *J. Neurosci.* 16:4983–4993.

39. Hess, P., J. B. Lansman, and R. W. Tsien. 1986. Calcium channel selectivity for divalent and monovalent cations. Voltage and concentration dependence of single channel current in ventricular heart cells. *J. Gen. Physiol.* 88:293–319.

40. Busselberg, D., D. Michael, M. L. Evans, D. O. Carpenter, and H. L. Haas. 1992. Zinc (Zn^{2+}) blocks voltage gated calcium channels in cultured rat dorsal root ganglion cells. *Brain Res.* 593:77–81.

41. Marcus, Y. 1994. A simple empirical-model describing the thermodynamics of hydration of ions of widely varying charges, sizes, and shapes. *Biophys. Chem.* 51:111–127.

42. Hefter, G., Y. Marcus, and W. E. Waghorne. 2002. Enthalpies and entropies of transfer of electrolytes and ions from water to mixed aqueous organic solvents. *Chem. Rev.* 102:2773–2836.

43. Serrano, J. R., S. R. Dashti, E. Perez-Reyes, and S. W. Jones. 2000. Mg^{2+} block unmasks Ca^{2+}/Ba^{2+} selectivity of alpha1G T-type calcium channels. *Biophys. J.* 79:3052–3062.

44. Krovetz, H. S., H. M. VanDongen, and A. M. VanDongen. 1997. Atomic distance estimates from disulfides and high-affinity metal-binding sites in a K^+ channel pore. *Biophys. J.* 72:117–126.

45. Backx, P. H., D. T. Yue, J. H. Lawrence, E. Marban, and G. F. Tomaselli. 1992. Molecular localization of an ion-binding site within the pore of mammalian sodium channels. *Science.* 257:248–251.

46. Tufty, R. M., and R. H. Kretsinger. 1975. Troponin and parvalbumin calcium binding regions predicted in myosin light chain and T4 lysozyme. *Science.* 187:167–169.

47. da Silva, A. C., and F. C. Reinach. 1991. Calcium binding induces conformational changes in muscle regulatory proteins. *Trends Biochem. Sci.* 16:53–57.

48. Doughty, S. W., F. E. Blaney, B. S. Orlek, and W. G. Richards. 1998. A molecular mechanism for toxin block in N-type calcium channels. *Protein Eng.* 11:95–99.

49. Feng, Z. P., J. Hamid, C. Doering, G. M. Bosey, T. P. Snutch, and G. W. Zamponi. 2001. Residue Gly1326 of the N-type calcium channel alpha 1B subunit controls reversibility of omega-conotoxin GVIA and MVIIA block. *J. Biol. Chem.* 276:15728–15735.

50. Kang, H. W., J. Y. Park, S. W. Jeong, J. A. Kim, H. J. Moon, E. Perez-Reyes, and J. H. Lee. 2006. A molecular determinant of nickel inhibition in $Ca_V3.2$ T-type calcium channels. *J. Biol. Chem.* 281: 4823–4830.